# Supplementary material
# Mesoscopic transport in electrostatically-defined spin-full channels in quantum Hall ferromagnets

Aleksandr Kazakov, George Simion, Yuli Lyanda-Geller, Valery Kolkovsky,
Zbigniew Adamus, Grzegorz Karczewski, Tomasz Wojtowicz, and Leonid P. Rokhinson

## CONTENTS



## S1. AFM IMAGES OF SAMPLES

Images of constrictions with the gate boundaries are shown in Fig. S1. Numbers indicate lithographical width of constrictions along gate boundaries.

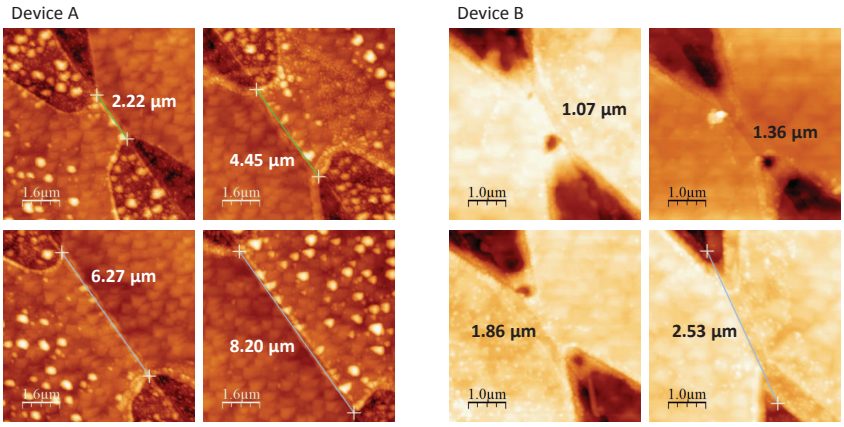


FIG. S1. AFM micrographs of Devices A and B. A faint line across the constriction is the Ti gate boundary.

## S2. 2DEG PREPARATION

We found that conditions of LED illumination have a great impact on the width and electrostatic control of the QHFm transition. Illumination of a sample with a red LED at ∼10 K results in a very wide $(0.5-0.8$ T) QHFm transition which has a position that is sensitive to the gate voltage ($0.3-0.4$ T per 100 V on a back gate voltage). Similar results were obtained by illuminating a sample with a green LED at low temperatures ∼ 200 mK. Illumination with a green LED at high temperatures (∼10 K) results in a 2D gas with ∼ 30% higher carrier density and narrow $(0.1-0.3$ T) QHFm transition with a position almost insensitive to the applied gate voltage.

The optimal QHFm transition width and gate sensitivity was achieved by illuminating samples with a green LED at low temperatures and subsequent heating to 1 K, where after 2-4 hours the 2D gas relaxed into an intermediate state with a $0.2-0.4$ T - wide QHFm transition and $0.1-0.2$ T/100 V transition control. Thus, prepared 2D gases vary slightly between cooldowns for the same sample and between different samples.

The Ti front gate, evaporated directly on the CdTe surface, is found to modify surface pinning potential and reduce electron density under the gate by a factor of 2, see Fig.S2. Modified surface pinning potential causes different dopant ionization profiles and, consequently, different profile of the electron wavefunction within the quantum well. This difference allowed us to adjust the transition field $B^*$ at zero gate voltage by varying conditions of the LED illumination during a cooldown. Sharp peaks near 3.5 T and 7 T are QHFm transitions due to Landau level crossings. Adjusting front and back gate voltages we can position the 7 T QHFm transition between $|1\downarrow\rangle$ and $|0\uparrow\rangle$ states within the $\nu = 2$, as shown in the middle and bottom panels in Fig. S2.

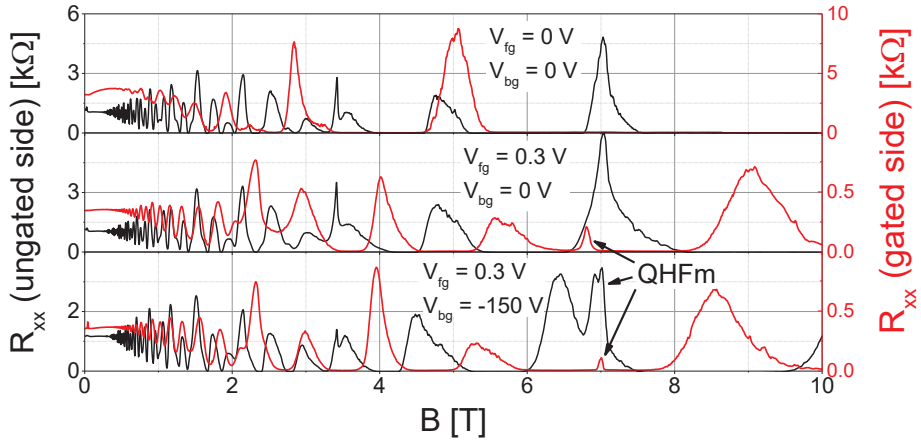


FIG. S2. After cooldown densities under gate and outside the gate differ by a factor of 2-3 due to surface Fermi level pinning by the gate. In order to align densities one needs to apply a high voltage on the front gate. After aligning densities and placing $\nu = 2$ in the vicinity of the QHFm transition one can observe QHFm transitions on both ungated and gated sides.

## S3. CHARACTERIZATION OF LOCAL HEATING BY EXCITATION CURRENT

Current dependence of $R_{DW}$ measured at base $T < 30$ mK is shown in Fig.S3. Saturation of $R_{DW}$ at low currents indicates that for excitation currents $I_{ac} < 1$ nA Joule heating is negligible.

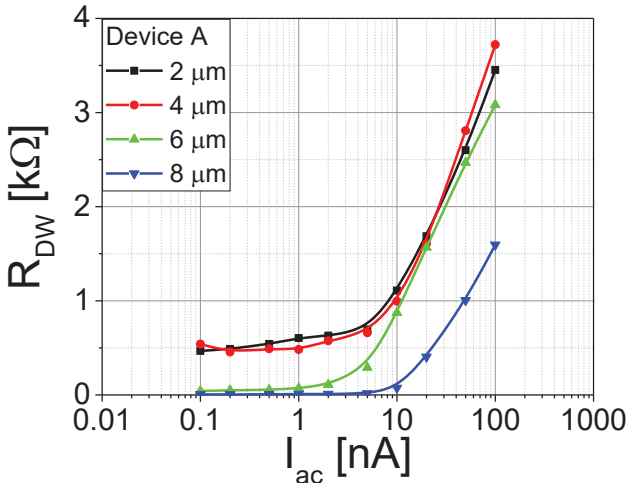


FIG. S3. Dependence of $R_{DW}$ for different channel lengths on excitation current at a base temperature $T = 27$ mK.

## S4. MODELING LONGITUDINAL RESISTANCE IN THE PRESENCE OF A DOMAIN WALL

Multi-terminal transport in the quantum Hall effect regime can be accurately modeled within a Landauer-Büttiker formalism. First, let us calculate the longitudinal resistance in a sample with variable electron density, across a chiral edge state formed at the density boundary, see Fig.S4(a). We have a sample with four contacts and two areas of different filling factors ($\nu = n$ and $\nu' = n+1$). In this case if we would pass current $i$ from source contact **1** to drain contact **2** the measured voltage drop between contacts **3** and **4** can be found from solving a set of Kirchhoff's equations:

$$\begin{cases} (n+1) * g_0 * V_4 - (n+1) * g_0 * V_1 + i = 0 \\ V_2 = 0 \\ n * g_0 * V_2 - n * g_0 * V_3 = 0 \\ n * g_0 * V_3 + g_0 * V_1 - (n+1) * g_0 * V_4 = 0 \end{cases} . \tag{S1}$$

Here $g_0$ is the quantum conductance $\frac{e^2}{h}$. The resistance across the chiral edge state $R_{ch}$ is

$$R_{ch} = \frac{V_4 - V_3}{i} = \frac{1}{n(n+1)} \frac{1}{g_0} = \frac{1}{n(n+1)} \frac{h}{e^2}. \tag{S2}$$

This result was obtained for one magnetic field direction. Magnetic field reversal would flip the direction of propagation of the edge states. By rewriting the system of equations one can find potentials of contacts **3** and **4**. They are the same $V_3 = V_4 = \frac{i}{g_0 n}$. Thus, in reversed magnetic field $R_{ch} = 0$.

Now we turn to the modeling of resistance in the presence of a hDW at $\nu = 2$. First, we consider the case of two non-interacting counterpropagating edges with no inter-scattering and no equilibration between $\nu = 2$ and $\nu = 1$ edge states, Fig.S4(b). The solution is $R_{DW} = \frac{V_4 - V_3}{i} = \frac{1}{2} \frac{h}{e^2}$=12.9 kΩ, independent of field direction.

Analyzing resistivity of the domain wall constriction, we consider two possibilities. The first is the inter-edge scattering between counterpropagating edge states along the gate boundary. In

this case, we parametrize the domain wall resistance by a finite conductivity $g = 1/r$ between edge channels, Fig.S4(c). The system of Kirchhoff's equations for this case is:

$$\begin{cases} 2 * g_0 * V_4 - 2 * g_0 * V_1 + i = 0 \\ g_0 * V_1 - g_0 * V_a + g * (V_b - V_a) = 0 \\ g_0 * V_3 - g_0 * V_b - g * (V_b - V_a) = 0 \\ V_2 = 0 \\ 2 * g_0 * V_2 - 2 * g_0 * V_3 = 0 \\ g_0 * V_a + g_0 * V_3 - 2 * g_0 * V_4 = 0 \end{cases}, \tag{S3}$$

and $R_{DW} = \frac{r+1}{2r+6}\frac{h}{e^2}$, Fig.S4(e). While the value $1/6 < R_{DW} < 1/2$ depends on $r$, it is inconsistent both with the value of resistance and with dependence of resistance on the length of the hDW channel observed experimentally. Indeed, interedge scattering would mostly depend on the width of the channel, and will not exhibit exponential dependence on its length.

A hDW formed from fully hybridized counter-propagating edges is modeled as a single channel with conductivity $g = 1/r$ connecting $\nu = 2$ edge states on the opposite sides of the sample, Fig.S4(d). In this case Kirchhoff's equations are:

$$\begin{cases} 2 * g_0 * V_4 - 2 * g_0 * V_1 + i = 0 \\ g_0 * V_1 - g_0 * V_a + g * (V_b - V_a) = 0 \\ V_2 = 0 \\ 2 * g_0 * V_2 - 2 * g_0 * V_3 = 0 \\ g_0 * V_3 - g_0 * V_b - g * (V_b - V_a) = 0 \\ g_0 * V_b + g_0 * V_3 - 2 * g_0 * V_4 = 0 \end{cases}, \tag{S4}$$

and in this case $R_{DW} = \frac{1}{4r+6}\frac{h}{e^2}$, Fig.S4(f). Experimentally observed resistance is consistent with this picture and the theoretical model of conduction through in-gap states is discussed in Section S9. By substituting $r \to \infty$, this case corresponds to an insulating hDW and is reduced to the usual quantum Hall case with $R_{xx} = 0$. This situation was observed for long hDW, longer than 6-8 $\mu$m.

We note that in the case of a highly conducting hDW, $r \to 0$, we get $R = \frac{1}{6}\frac{h}{e^2}$ as in the previous case, Fig.S4(c,e). For models Fig.S4(c,d) with $r \to 0$ it is easy to show that the corresponding systems of equations are the same. Physically it means that points **a** and **b** have the same potential and can be merged together on Figs.S4(c,d). It's easy to show that for all hDW models $R_{DW}(B) = R_{DW}(-B)$, reflecting the fact that hDWs are symmetric under B-field inversion.

## S5. DEPENDENCE OF CONDUCTANCE FLUCTUATIONS ON $\Delta B^*$

Separation of QHFm transitions in gated and ungated regions $\Delta B^*$ reflects the value of the s-d exchange gradient near the gate boundary and, as a result, positions of ferromagnetic domains. For $\Delta B^* = 0$ there is no s-d exchange gradient and domains are randomly formed within the 2D plane. Narrow field sweeps within $7.3\ T < B < 7.5\ T$ range across the QHFm transition results in the formation of different domain configurations, different conduction paths, and different patterns of conduction fluctuations, Fig. S5(a). Often there is no domain wall formed in the vicinity of the constriction, in this case no conduction is observed as shown for the up-sweep in (a). In contrast, for $\Delta B^* = 0.2$ T the gate-induced s-d exchange gradient stabilizes the domain wall position and

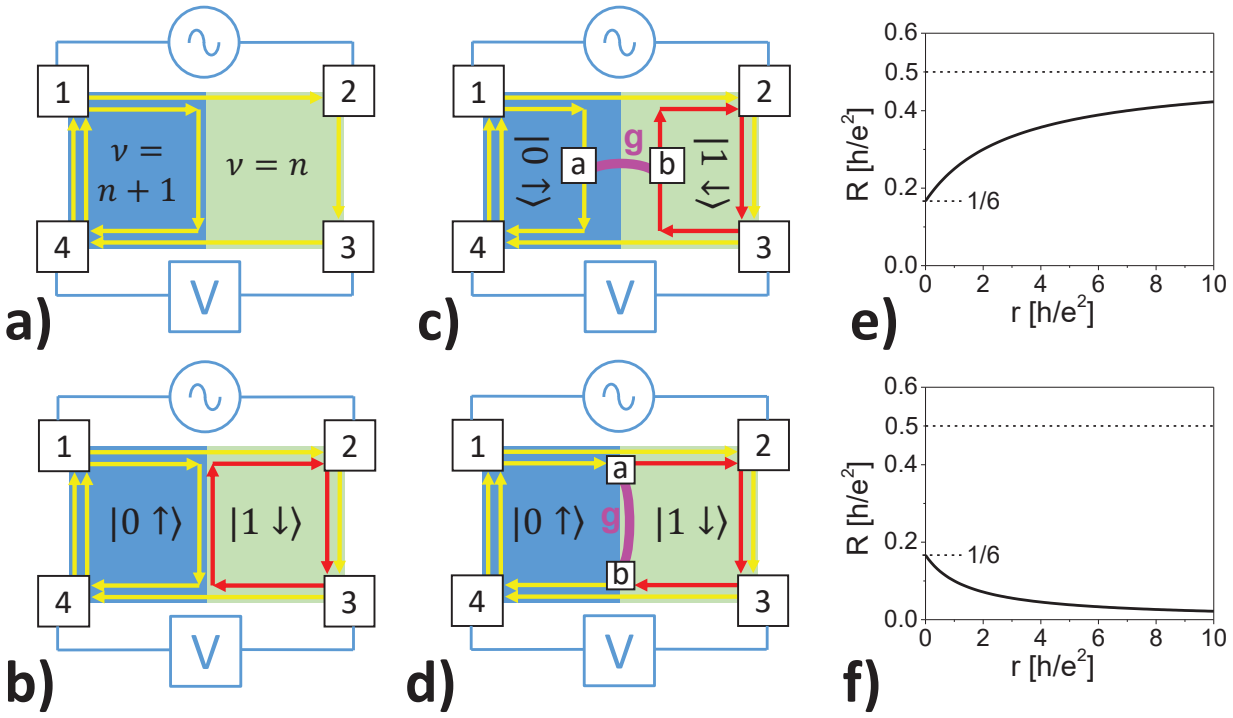


FIG. S4. (a) Edge states in a sample with different filling factors. (b) Edge states at the domain boundary in the absence of inter-edge scattering. (c) The same with inter-edge scattering $g$ or (d) formation of a hDW with conduction $g$. (e,f) Dependence of longitudinal resistance $R$ on conduction $g = 1/r$ calculated for models (c,d).

conducting channels are always formed. The conduction channel is well defined and the resistance fluctuation pattern is reproducible over multiple field sweeps, Fig. S5(b).

## S6. TIME EVOLUTION OF MESOSCOPIC FLUCTUATIONS

Even for large QHFm transition separation $\Delta B^* = 0.2$ T and at the lowest $T < 30$ mK there is a slow change in the pattern of resistance fluctuations with time, Fig. S6. A characteristic time scale for the pattern change is $\sim 7$ hours, as determined from a half width at the half height of the autocorrelation function $F(\Delta t) = \langle R_{DW}(t) R_{DW}(t + \Delta t) \rangle$. Most likely the conduction path and the fluctuation pattern are affected by gate voltage-induced slow motion of localized charges in the vicinity of the conduction channel.

## S7. DEPENDENCE OF HELICAL CHANNEL CONDUCTANCE ON THE POSITION OF $B^*$ WITHIN THE $\nu = 2$ PLATEAU

The value of the maximum conductivity of the channel (which corresponds to the maximum of $R_{DW}$) formed between states with opposite spin polarization depends not only on the length of the channel and QHFm separation $\Delta B^*$, but also on the position of the QHFm transition within the $\nu = 2$ plateau. In Fig. S7 we simultaneously change density in gated and ungated regions and sweep the QHFm in the channel $\langle B^* \rangle = (B^*_{gated} + B^*_{ungated})/2$ across the $\nu = 2$ plateau while keeping $\Delta B^*$ approximately constant. Magnetoresistance in the gated and ungated regions is plotted in

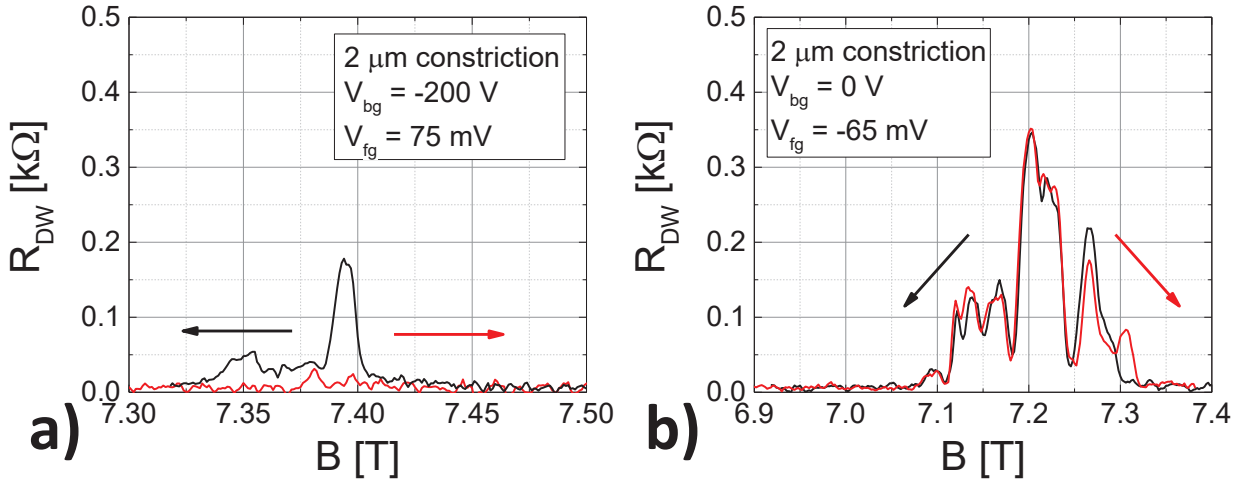


FIG. S5. Mesoscopic resistance fluctuations for 2 $\mu$m channels are shown for (a) $\Delta B^* = 0$ and (b) $\Delta B^* = 0.2$ T. For each temperature point consecutive $B$-scans in both field directions were recorded.

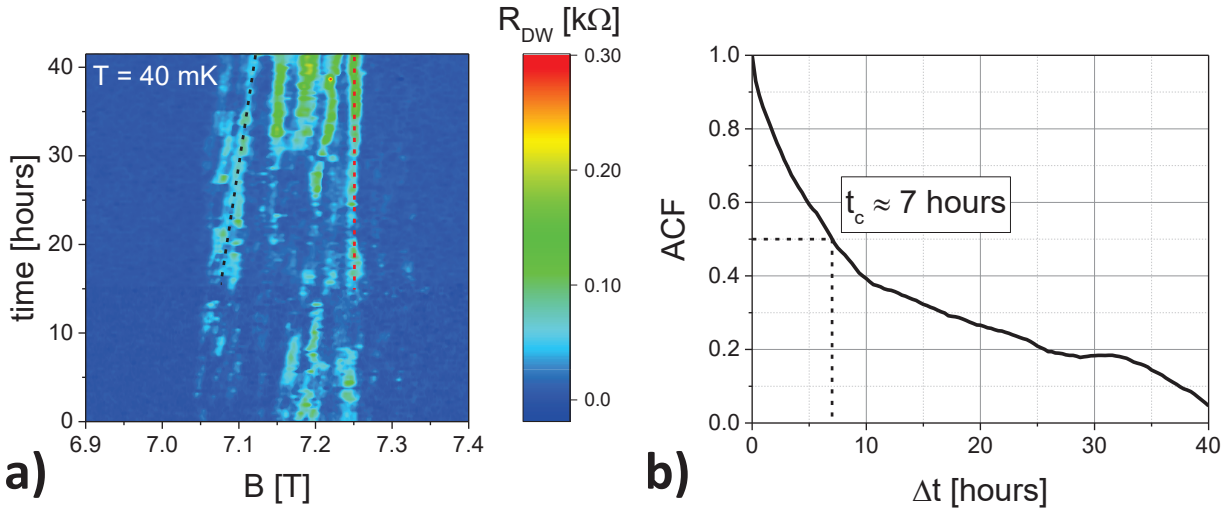


FIG. S6. Time evolution of resistance fluctuations in a 2 $\mu$m channel is plotted in the color plot for $\Delta B^* = 0.2$ T and $T = 40$ mK. Data was recorded for $B = 6.9\ T \rightarrow 7.4\ T$ sweeps. (b) Resistance auto-correlation function as a function of time offset $\Delta$t.

the left plot, and across the 2 $\mu$m constriction in the right plot, Fig.S7. In the inset, the resistance saturation value $R_0$ and activation energy $E_a$ are extracted from the temperature dependence of $R_{DW}$. It is clear that extrema of $R_0$ and $E_a$ depend on the position of $\langle B^* \rangle$ within the $\nu = 2$ plateau, with the minimum $R_0$ and the maximum $E_a$ occur at $\nu = 2$. The data discussed in the main text is taken for $\langle B^* \rangle$ placed close to the center of the $\nu = 2$ plateau in both gated and ungated regions.

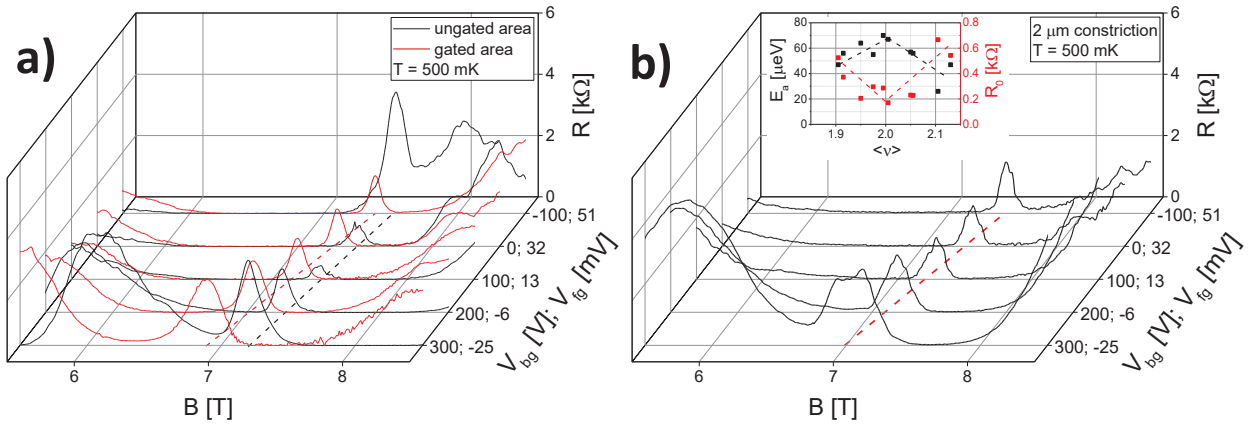


FIG. S7. $R_{DW}$ in the vicinity of the $\nu = 2$ QHE state is plotted for gated and ungated regions (left) and across a 2 $\mu$m constriction for different front gate $V_{fg}$ and back gate $V_{bg}$ voltages at $T = 500$ mK. Here position of the QHFm transition $\langle B^* \rangle$ is shifting relative to the center of the $\nu = 2$ plateau in both gated and ungated regions. In the inset the value of saturation resistance $R_0$ and activation energy $E_a$ are plotted as a function of a filling factor of $\langle B^* \rangle$, where $R_0$ and $E_a$ are extracted from the constant + activation function fits to the temperature dependence of QHFm transition peaks.

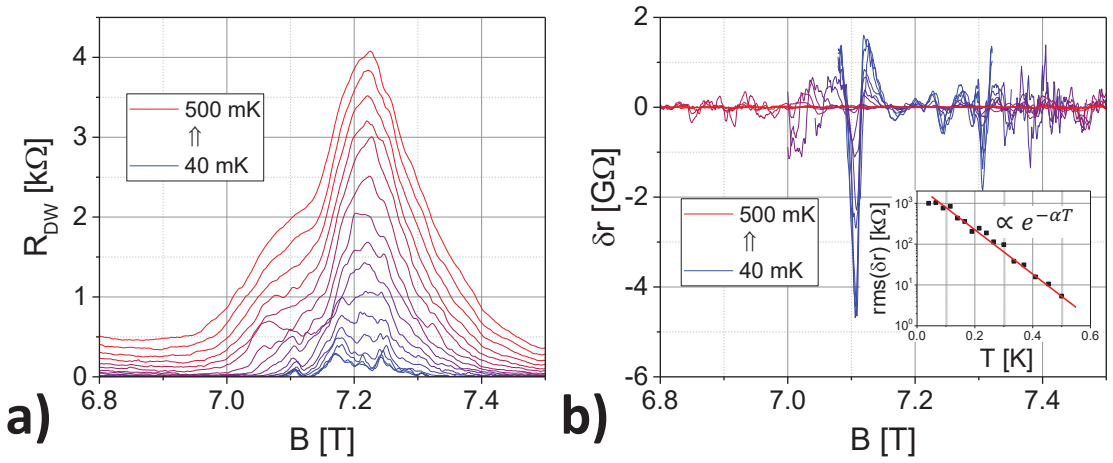


FIG. S8. (a) Resistance $R_{DW}$ across 2 $\mu$m constriction at different temperatures. (b) Corresponding fluctuations $\delta r$ of resistance r along the gate boundary. Inset shows standard deviation of resistance across a 2 $\mu$m constriction.

## S8. TEMPERATURE DEPENDENCE OF RESISTANCE FLUCTUATIONS AND THE PHASE COHERENCE LENGTH

Temperature dependence of resistance fluctuations across a 2 $\mu$m constriction is shown in Fig. S8a, where the magnetic field was swept in a narrow range near the the QHFm transition (6.8-7.5 T) in order to preserve the fluctuation pattern. The channel resistance $r$ can be calculated from the measured resistance $R_{DW}$ using Landauer-Büttiker formalism discussed earlier:

$$r = \frac{1 - 6R_{DW}}{4R_{DW}}, \tag{S5}$$

where both $r$ and $R_{DW}$ are expressed in units of $h/e^2$. Fluctuations of the measured resistance $\delta R_{DW}$ are obtained by subtracting a smooth background from the resistance $R_{DW}$, and fluctuations of the resistance of the conducting channel $\delta r$ are calculated as

$$\delta r = \frac{dr}{dR_{DW}}\delta R_{DW} = -\frac{1}{4}\frac{\delta R_{DW}}{R^2}. \tag{S6}$$

Extracted fluctuations of channel resistance are plotted in Fig. S8b for a wide temperature range. In the inset rms amplitude of $\delta r$ is plotted as a function of temperature. From exponential decay of rms($\delta r$) with temperature $rms \propto e^{-T_0/T} = e^{-L/l_\phi(T)}$, $T_0 = 80$ mK, we estimate that phase coherence length $l_\phi$ exceeds $\approx 800$ nm below 100 mK for $L \approx 1$ $\mu$m. Thus the phase coherence is preserved over the length of the channel.

## S9. MODELING OF DOMAIN WALL CONDUCTION IN THE QHFM REGIME

In order to model our system, we consider $N$ electrons confined to a $L_x \times L_y$ rectangle, subjected to a magnetic field $B = -B\hat{e}_z$. We take $N = [\nu L_x L_y/2\pi\ell^2]$, where $\ell$ is the magnetic length and $\nu = 2$ is the filling factor.

$$\begin{aligned} H_s = \sum_i \Big[ & \frac{1}{2m^*}\left(\mathbf{p}_i + \frac{e\mathbf{A}}{c}\right)^2 + \frac{\beta_R}{\hbar}\left(\mathbf{p}_i\frac{e\mathbf{A}}{c}\right) \times \boldsymbol{\sigma}_i \\ & + V_G(\mathbf{r})\sigma_{z,i} + V_{\rm imp}(\mathbf{r}) + V_{\rm fl}^{\rm mag}(\mathbf{r})\sigma_z\Big] \\ & + \frac{e^2}{2\epsilon_r}\sum_{i,j}\frac{1}{|\mathbf{r}_i - \mathbf{r_j}|} \end{aligned} \tag{S7}$$

Here $m^* = 0.1m$ is the effective electron mass in CdTe and $\beta$ is the Rashba constant. The spin dependent potential $V_G$ mimics variation of the Zeeman energy across the sample as a result of

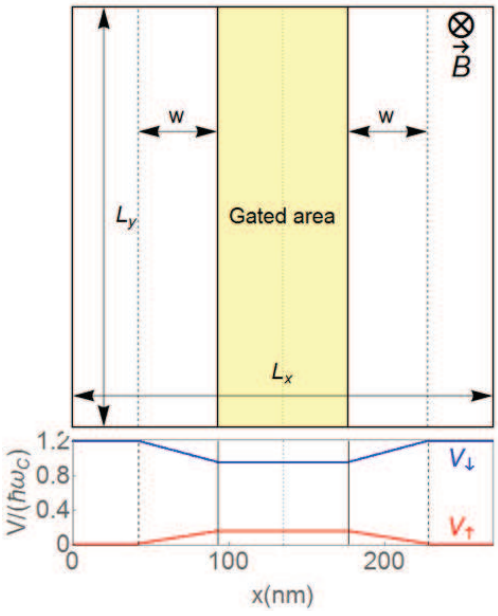


FIG. S9. Schematic view of the simulated system and the spin dependent potential due to gate voltage.

applied gate voltage. We consider a remote impurity potential $V_{\rm imp}(\mathbf{r}) = \sum_i^{N_i} w_i \exp[-(\mathbf{r}-\mathbf{r_i})^2/d^2]$, where the number of impurities $N_i = N$ and $r_i$'s denote the position of the randomly placed impurities in the doping layer and $w_i \in [-W, W]$. Surface roughness (see Fig. 6(e) of the main text) translates into a curvy profile of the quantum well, and as a consequence, into the deviation of magnetic field orientation. This deviation causes fluctuations of Mn spin orientation from the z-direction. In order to model this effect of surface roughness we introduce the spin dependent random potential $V_{\rm fl}^{\rm mag}({\rm r}) = \sum_i u_i \exp[-(\mathbf{r}-\mathbf{r}_i)^2/b^2]\sigma_z$. We choose $W = 8$ meV, $d = 40$ nm, and $u = 15$ $\mu$eV and $b = 150$ nm. Parameters for remote dopants are chosen to be consistent with the electron mobility that has been measured experimentally ($\mu = 30,000$ cm/Vs at $B = 0$). The electron-electron interaction is taken into account using the Hartree-Fock approximation. The self-consistent procedure is done in the basis set of five orbital Landau states, each with two spin projections. In our numerical procedure, the spin-dependent potential and random impurities are chosen to be symmetric with respect to the reflection about a line parallel to the $y$-axis that bisects $L_x$; $V_G(x, y) = V_G(L_x - x, y)$ and $x_{N/2+i} = L/2 - x_i$, $y_{N/2+i} = y_i$. Periodic boundary conditions are used in both $x$ and $y$ directions. The Hartee-Fock procedure reduces the Hamiltonian to a non-diagonal and non-local effective single particle form [1].

This model yields two counterpropagating edge channels experiencing avoided crossing due to the spin-orbit gap. Impurities provide states in the gap mediating the conduction in short channels. We compute the conductance of our finite system using a Green's function approach [2]. Knowing the single particle Hartree-Fock and impurity potential, we discretize the problem on a lattice of $N_x \times N_y$ points. We place our leads in the channels separated by $L_y/2$. The Hamiltonian describing the system with leads is given by

$$H_t = H_s + H_1 + H_2 + V_{1s} + V_{2s} \ , \tag{S8}$$

where $H_i$ describes the lead, $V_{is}$ is the coupling between lead and the localized electron states in the domain wall area ($i = 1, 2$ label the lead). The conductance is given by

$$G = \frac{e^2}{h} {\rm Tr}\left(\hat{\Gamma}_1 \hat{\mathcal{G}_R} \hat{\Gamma}_2 \hat{\mathcal{G}_A}\right) \ , \tag{S9}$$

where $\mathcal{G}_{R/A}$ denotes the retarded (advanced) Green's function of the interacting electron gas, $\hat{\mathcal{G}}_{A,R} = [(E \pm i\eta)\hat{I} - \hat{H}]^{-1}$, $E$ is the energy (we take $E = E_F$), $\hat{\Gamma}_i = i(\hat{\Sigma}_i^R - \hat{\Sigma}_i^A)$ are the coupling matrices, and the contact retarded and advanced self-energies $\hat{\Sigma}_i^R$ and $\hat{\Sigma}_i^A$ are given by

$$\hat{\Sigma}_i^R = V_{is}^\dagger \left[(E + i\eta)\, \hat{I} - \hat{H}_i\right]^{-1} \hat{V}_{is} \tag{S10}$$

$$\hat{\Sigma}_i^A = V_{is}^\dagger \left[(E - i\eta)\, \hat{I} - \hat{H}_i\right]^{-1} \hat{V}_{is} \ . \tag{S11}$$

We compute the conductance using (S9) and extract the conductivity of the hDW $\sigma_{yy}$. When both magnetic and remote impurities are present, the averaged conductivity for five realizations of disorder is found to be $1/r = \sigma_{yy} = 0.146 \pm 0.023$ $\frac{e^2}{h}$. If magnetic fluctuations are ignored, we obtain $\sigma_{yy} = 0.105 \pm 0.018$ $\frac{e^2}{h}$. The calculated value $\sigma_{yy} = 0.146$ $\frac{e^2}{h}$ corresponds to the channel resistance $r = 1/\sigma_{yy} = 177$ k$\Omega$ or $R_{DW} = 0.77$ k$\Omega$. This value of $R_{DW}$ is in good agreement with the measured resistance $R_{DW} = 0.66 - 0.87$ $k\Omega$, suggesting that the model captures the essential physics of conduction in the channels formed along domain walls. In-gap states naturally provide conduction channels for electrons propagating in both directions. Therefore, the system yields resistivity $R_{DW}$ symmetric under magnetic field direction reversal, in agreement with experiment.

[1] Giuliani G. and Vignale G., *Quantum Theory of the Electron Liquid* (Cambridge University Press, 2005).

[2] Ferry D.K., Goodnick S.M., and Bird J., *Transport in Nanostructures* (Cambridge University Press, 2009).